

# Robust intrinsic half-metallic ferromagnetism in stable 2D single-layer $\text{MnAsS}_4$

Tengfei Hu, Wenhui Wan, Yanfeng Ge and Yong Liu

State Key Laboratory of Metastable Materials Science and Technology & Key Laboratory for Microstructural Material Physics of Hebei Province, School of Science, Yanshan University, Qinhuangdao 066004, China

E-mail: yongliu@ysu.edu.cn, ycliu@ysu.edu.cn

February 2020

**Abstract.** Two-dimensional (2D) intrinsic half-metallic materials are of great interest to explore the exciting physics and applications of nanoscale spintronic devices, but no such materials have been experimentally realized. Using first-principles calculations based on density-functional theory (DFT), we predicted that single-layer  $\text{MnAsS}_4$  was a 2D intrinsic ferromagnetic (FM) half-metal. The half-metallic spin gap for single-layer  $\text{MnAsS}_4$  is about 1.46 eV, and it has a large spin splitting of about 0.49 eV in the conduction band. Monte Carlo simulations predicted the Curie temperature ( $T_c$ ) was about 740 K. Moreover, Within the biaxial strain ranging from -5% to 5%, the FM half-metallic properties remain unchanged. Its ground-state with 100% spin-polarization ratio at Fermi level may be a promising candidate material for 2D spintronic applications.

*Keywords:* First-principles calculations, 2D materials, half-metallic, spintronics

## 1. Introduction

Spintronics, which uses the spin of electrons for the information storage, transport and processing, have attracted intensive interests from the viewpoint of fundamental science and technology applications in the past decades [1]. It is important in the field of quantum computing and the next-generation information technology [2,3]. Half-metallic materials, which is conducting in one spin orientation but insulating in the opposite spin direction meet the demand of a 100% spin polarization ratio, are highly desirable for advanced spintronic applications [4]. The band gap for the insulating channel is termed as spin gap. To prevent spin leakage, the spin gap needs to be as wide as possible [5]. Since the first half-metallic material NiMnSb was predicted in 1983 [6], there has been a flurry of research into magnetic half-metals, such as transition metal compounds  $\text{MnX}$  ( $X = \text{P, As}$ ),  $\text{NbF}_3$ ,  $\text{CoH}_2$ ,  $\text{ScH}_2$ ,  $\text{TiCl}_3$ ,  $\text{VCl}_3$  [7–10]; sp half-metallic ferromagnets  $\text{RbSe}$  and  $\text{CsTe}$  [11–14].

Although half-metallic material has been studied for a long time, the demonstrated half-metals was very limited and have serious shortcomings, such as high cost or low  $T_c$ .

Until now, intrinsic half-metallic material with wide spin gap and high  $T_c$  is still absent in experiments. However, the single-layer CrPS<sub>4</sub> [15] is predicted to be a ferromagnetic semiconductor and the valence bands are split for different spin orientation. As hole doping can lower Fermi level into the valence bands of one spin and lead to half-metallic ferromagnets [16, 17]. An obvious option is to replace Cr by Mn atoms, and by stability calculation we replace P with As atoms.

In this paper, the first-principles calculations are used to investigate the mechanical, dynamical, electronic and magnetic properties of single-layer MnAsS<sub>4</sub>. Our calculations indicate that the MnAsS<sub>4</sub> crystal is mechanically and dynamically stable, so it is possibly prepared. It is metallic at the Fermi level in one spin direction and has a band gap of 1.46 eV in the opposite spin direction. Its half-metallic properties do not change under the biaxial strain range from -5% to 5%. It has stable ferromagnetism phase with integer magnetic moment of  $8 \mu_B$  per primitive cell. Furthermore, we demonstrated that the MnAsS<sub>4</sub> exhibits high  $T_c$  about 740 K.

## 2. Methods

Kohn-Sham DFT calculations are performed using the projector augmented wave method, as implemented in the plane-wave code VASP [18–20]. A cutoff energy of 500 eV and a Monkhorst-Pack special k-point mesh [21] of  $17 \times 19 \times 1$  for the Brillouin zone integration was found to be sufficient to obtain the convergence. We used a Perdew-Burke-Ernzerhof (PBE) type generalized gradient approximation (GGA) in the exchange-correlation functional [22]. A conjugate-gradient algorithm was employed for geometry optimization using convergence criteria of  $10^{-7}$  eV for the total energy and 0.005 eV/Å for Hellmann-Feynman force components. We used GGA+U to treat the strong on-site Coulomb interaction [23]. A series of U values were selected, that is, 1.0-6.0 eV for Mn. Whatever U was, it didn't affected the ground-state of MnAsS<sub>4</sub>. Thus, whatever U were, the main conclusions were the same. So we displayed that results with Hubbard U term 5 eV for Mn [24] as suggested by Dudarev *et al* [25]. The band structures for different U values can be found in Figure A1. Phonon dispersions were calculated by density functional perturbation theory [26] by the Phonopy package interfaced to VASP code with  $2 \times 2 \times 1$  supercell. We inserted a 15 Å vacuum slab to avoid the interactions between periodic images.

## 3. Results and discussion

The atomic structure of single-layer MnAsS<sub>4</sub> is shown in Figure 1. The unit cell has parameters  $a = 11.34 \text{ \AA}$ ,  $b = 7.89 \text{ \AA}$  (Figure C1) and space group  $C_{2/m}$ . As shown in Figure 1(b), the As atoms bridge the twisted MnS<sub>6</sub> octahedral chain, according to the crystal field theory, 3d orbitals of a metal ion in an octahedral ligand perturbation field split into  $t_{2g}$  and  $e_g$  orbitals, the ground electron configuration of Mn<sup>3+</sup> ( $t_{2g}^3$  and  $e_g^1$ ) leads to a half-metallic character. A Mn atom connects six S atoms, three types

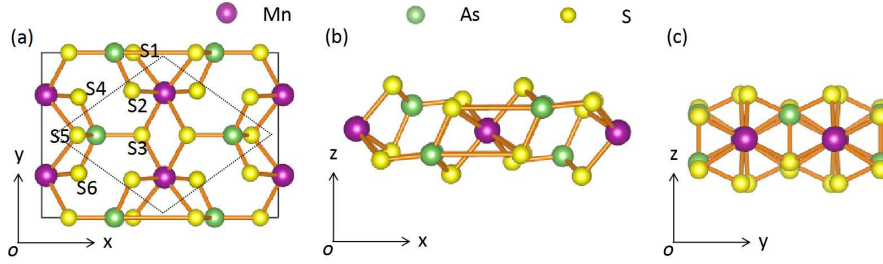


Figure 1: (Color online) The crystal structure of single-layer MnAsS<sub>4</sub> as seen from the (a) z-direction, (b) y-direction and (c) x-direction. The primitive cell is indicated by dotted line and the unit cell is indicated by solid line in (a).

of bond lengths of Mn-S1, Mn-S2, Mn-S3 are 2.635Å, 2.451Å and 2.646Å, respectively. An As atom connects four S atoms and the bond lengths of As-S3, As-S4, As-S5 are 2.198Å, 2.182Å and 2.214Å, respectively, and the As-S6 bond length is the same as As-S4. In the diamond box in Figure 1(a) is a primitive cell. A primitive cell contains two Mn atoms. We calculated that each primitive cell is an integer magnetic moment of  $8 \mu_B$ , and the local magnetic moment per Mn atom is about  $4 \mu_B$ , it is consistent with previous work [27, 28]

To determine the ground-state magnetic order, we compared the total energies of FM and different antiferromagnetic (AFM) structures [29]. The energy differences  $\Delta E$  relative to single-layer FM configurations are 170.69, 278.81, and 220.64 meV for the single-layer AFM1, AFM2, and AFM3 configurations, respectively. So the ground-state of single-layer MnAsS<sub>4</sub> is FM. Additionally, the non-magnetic (NM) state can be neglected owing to the great energy disparity between the NM state and magnetic states.

Table 1: Elastic constants  $C_{11}$ ,  $C_{12}$  and  $C_{22}$  (N/m) for single-layer MnAsS<sub>4</sub>.

$C_{11}$	$C_{12}$	$C_{22}$
76.69	10.39	71.35

Next, we determined its mechanical stability by calculating the three independent elastic constants. As shown in Table 1, we find that  $C_{11} = 76.69$  N/m,  $C_{12} = 10.39$  N/m and  $C_{22} = 71.35$  N/m, respectively. The elastic constants clearly satisfy Borns stability criterion [30], i.e.,  $C_{11} > 0$ ,  $C_{22} > 0$  and  $C_{11} - C_{12} > 0$ , indicating that they are mechanically stable. Meanwhile, we evaluate the stability of single-layer MnAsS<sub>4</sub> by comparing their binding energies, which is defined as

$$E_b = \frac{2E(Mn) + 2E(As) + 8E(S) - E(MnAsS_4)}{12},$$

where  $E(Mn)$ ,  $E(As)$ ,  $E(S)$  and  $E(MnAsS_4)$  are the energy of Mn atom, As atom, S atom and single-layer MnAsS<sub>4</sub>, respectively. According to this theory, the bigger  $E_b$  is,

the more stable the system will be. We find the binding energy is 4.03 eV per atom, which is bigger than the synthetic VI<sub>3</sub> [28] and others [31, 32].

In order to ensure the single-layer MnAsS<sub>4</sub> is dynamically stable, we calculated its phonon dispersion. As shown in Figure B1, the imaginary frequency is found to be absent in the whole Brillouin zone, it suggests that single-layer MnAsS<sub>4</sub> is dynamically stable and can exist as free-standing 2D crystal.

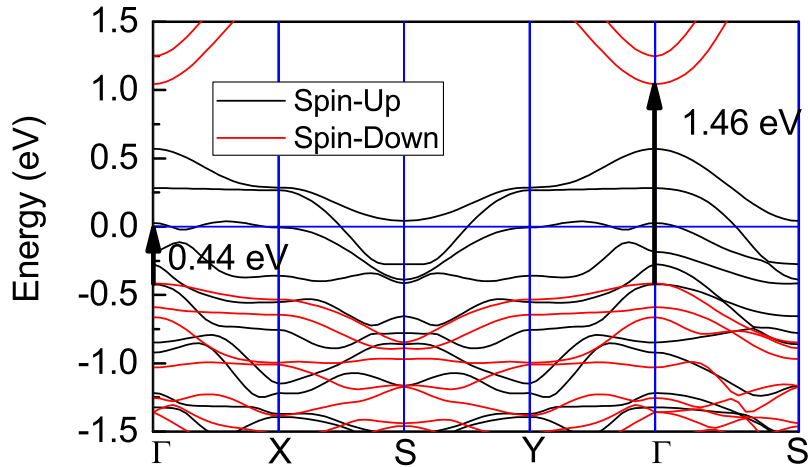


Figure 2: (Color online) Electronic band structures for single-layer MnAsS<sub>4</sub>.

Next, the electronic properties of single-layer MnAsS<sub>4</sub> were investigated. The band structures of single-layer MnAsS<sub>4</sub> are shown in Figure 2. Notably, the spin-up bands cross the Fermi level, while the spin-down channel acts as a semiconductor, indicating that it is intrinsic half-metallic material with 100% spin-polarization ratio. Comparing with previous studies where half-metallic materials occurred under certain external constraints, the half-metallic material found here is totally intrinsic, meaning that single-layer MnAsS<sub>4</sub> is more suitable for actual spintronic applications. As mentioned before, a wide half-metallic band gap and a wide spin gap are very important for half-metal in spintronic applications [33, 34]. Herein, the half-metallic band gap for single-layer MnAsS<sub>4</sub> is 0.44 eV, which is larger and smaller than the previous research on TiCl<sub>3</sub> (0.42 eV) and on VCl<sub>3</sub> (0.64 eV) [10]. The spin gap for the semiconducting channel is 1.46 eV, which is larger than the previous report of Fe<sub>2</sub>Si [35]. The wide spin gap and half-metallic gap make 2D MnAsS<sub>4</sub> an ideal candidate for miniaturized spintronic materials. Considering that, approximately 25%-45% of the spin gap is underestimated by DFT method [36], the spin gap of single-layer MnAsS<sub>4</sub> obtained by experiment may be larger than the above value. However, the trends of band dispersions and density of states are qualitatively reasonable, since we are mainly interested in their relative values, and the underestimate should not change the general trends of the results [37, 38].

Figure 3(a) shows the charge density difference of single-layer MnAsS<sub>4</sub>. It is the difference between the charge density at the bonding point and the atomic charge density at the corresponding point. The brown and green region represent the charge

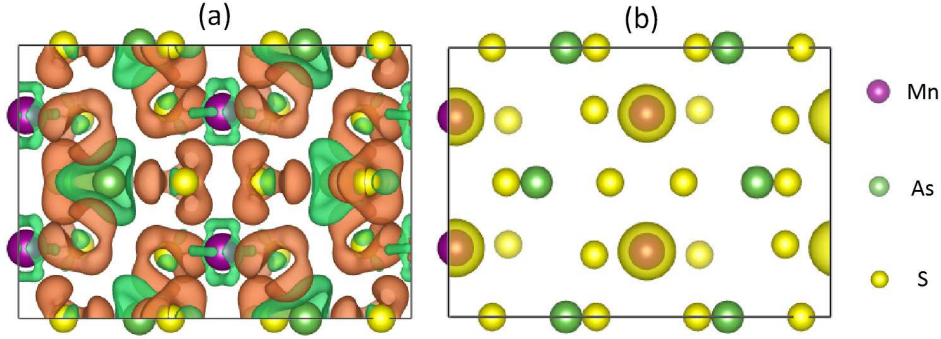


Figure 3: (Color online) (a) Charge density difference isosurface plot, showing charge accumulation and depletion (brown and green respectively). (b) Spin density isosurface plots for FM spin arrangements.

accumulation and depletion. It is obvious that Mn and As atoms lose electrons and S atoms gain electrons, due to that S atom has larger electronegativity. This allows Mn-S bonding to be more ionic. Figure 3(b) shows the spin density of single-layer  $\text{MnAsS}_4$ , we find that the induced spin polarization is mainly contributed by Mn atoms while the contribution from As and S atoms can be neglected, which is consistent with the magnetic moment analysis.

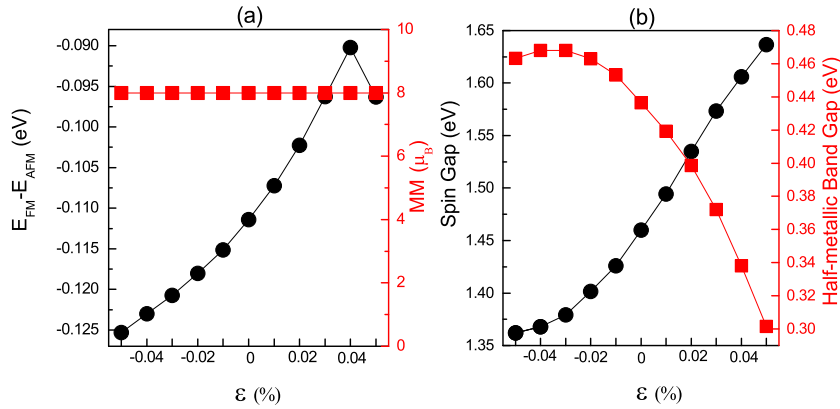


Figure 4: (Color online) Under biaxial strain for single-layer  $\text{MnAsS}_4$ . (a) Energy difference between the FM and AFM phases (black line) and total magnetic moments (red line). (b) Variation of the spin gap (black line) and half-metallic band gap (red line).

Figure 4(a) (red line) shows the change of total magnetic moment when a biaxial strain is applied. We find that the total magnetic moment is not affected when the biaxial strain range from -5% to 5%. Figure 4(a) (black line) shows the energy difference between FM and AFM configurations, and we can see that all values are negative, which

indicates that no phase transition occurs during the process of biaxial strain and FM is always ground-state. As shown in Figure 4(b) (black line), when the biaxial stretch occurs, the spin gap increases, but decreases when the biaxial compression. When the strain is 5%, the spin gap increases from 1.46 eV to 1.64 eV, and when the strain is -5%, the spin gap decreases to 1.36 eV, this trend is consistent with the previous report of  $\text{CrSiTe}_3$  [39]. When the biaxial strain of -3% is applied, the half-metallic band gap reaches the maximum value of 0.47 eV. When the biaxial strain is 5%, the half-metallic band gap is 0.30 eV.

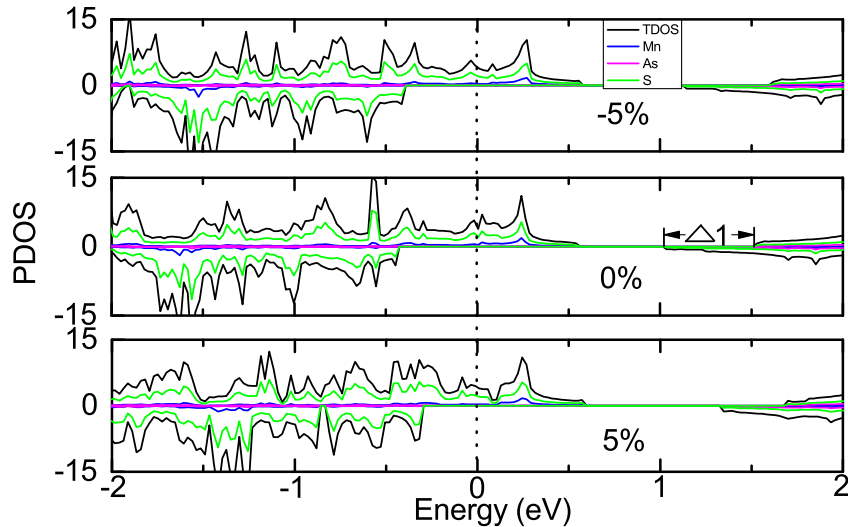


Figure 5: (Color online) Density of states for single-layer  $\text{MnAsS}_4$  under different biaxial strain. The percentage in the figure indicates the magnitude of the strain.

For the single-layer  $\text{MnAsS}_4$ , a large spin exchange splitting of 0.49 eV (labeled as  $\Delta_1$  in Figure 5) in the conduction band is observed, which is crucial for the application in spin-polarized carrier injection and detection [40]. When applying a biaxial strain of -5% and 5%, spin exchange splitting changes from 0.49 eV to 0.47 eV and 0.35 eV, respectively, which is larger than the  $\text{CrGeTe}_3$  (0.24 eV). Whether it is compressed or stretched, the density of states clearly shows that the contributions near the Fermi level are mainly from the Mn and S atoms.

Now, we turn our attention to the microscopic origin of the exchange interactions. Along the y direction, the distance between Mn atoms is too large ( $4.044\text{\AA}$ ) for the direct-exchange coupling to play an important role, the optimized Mn-S-Mn angle is  $99.6^\circ$ , which is near the ideal  $90^\circ$  bond angle.  $90^\circ$  bond angle usually associated with FM ordering and  $180^\circ$  associated with AFM ordering, according to the Goodenough-Kanamori rules [41,42], so it exhibits FM properties. Along the x direction, the exchange interactions are more indirect because the Mn-Mn distance is even larger ( $5.668\text{\AA}$ ). This indirect-exchange coupling is not only mediated by S atoms but also by As atoms, the optimized Mn-S-As, S-As-S, As-S-Mn angle is  $110.7^\circ$ ,  $120.2^\circ$ ,  $83.4^\circ$ , respectively. The transition crossover angle of FM-AFM is  $127 \pm 0.5^\circ$  [43], and the bond angle along the x direction are all smaller than  $127^\circ$ , so they prefer FM order. Therefore, the system

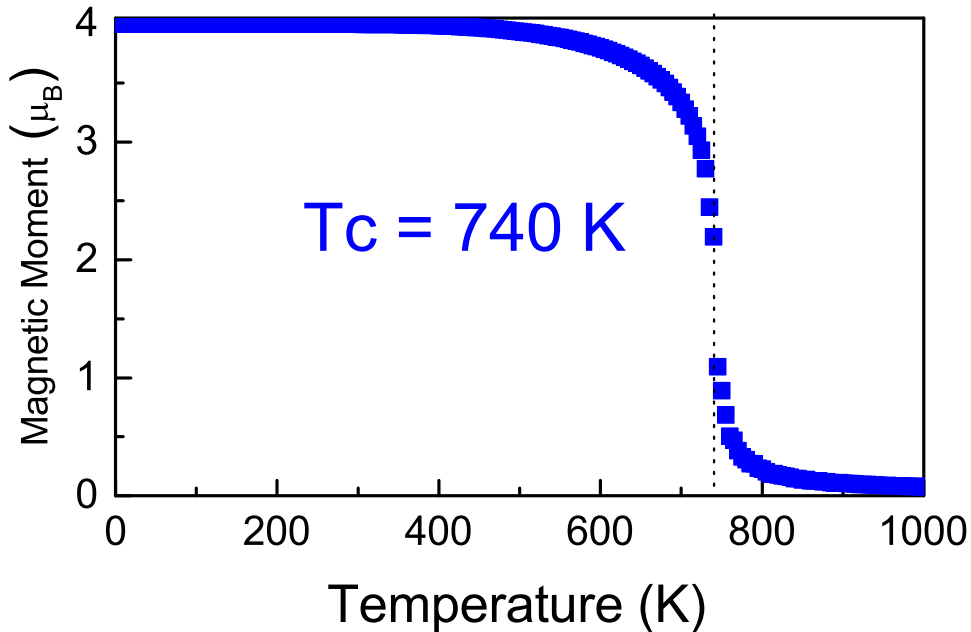


Figure 6: (Color online) Monte Carlo simulations on the average magnetic moment of Mn atoms for single-layer MnAsS<sub>4</sub> based on Ising model.

presents the FM ground-state.

To realize spintronic applications for single-layer MnAsS<sub>4</sub>, it is necessary to obtain the variation trend of local magnetic moment with  $T_c$ . We thus employed Monte Carlo simulations with the Hamiltonian  $H = - \sum_{\langle ij \rangle} J_{ij} S_i S_j$  to predict the FM transition temperature, where  $J_{ij}$  represents the exchange interactions of over all neighbor Mn-Mn pairs,  $S_i$  represents the spin of atom  $i$ . Herein we only consider nearest neighbors located along x and y directions. The exchange interaction parameters  $J_{ij}$  are determined by the relation between the total energy and spin configurations. Our result of total  $J_{ij}$  is 5.33 meV and 8.71 meV along the x and y directions, respectively,  $S=2$ . As shown in Figure 6, the  $T_c$  extracted from the figure is around 740 K. It is significantly higher than those reported before, e.g., CrI<sub>3</sub> monolayer (45 K) [44], CrSiTe<sub>3</sub> (35.7 K) and CrGeTe<sub>3</sub> (57.2 K) [40]

In similar structures, the AFM ground-state causes the energy band of spin-up and spin-down to coincide, which may lead to the formation of semiconductor materials. We predicted that the ground-state of MnSbS<sub>4</sub>, VPS<sub>4</sub> and CrAsS<sub>4</sub> is AFM, detailed studies focusing on the aspect might reveal some interesting physics.

#### 4. Conclusions

In summary, we presented an intrinsic ferromagnetic half-metallic material by using first-principles calculations. The calculations of mechanical properties, phonon dispersion and binding energy ensure the stability and the possibility of preparation of single-layer MnAsS<sub>4</sub>. The band structures show that the single-layer MnAsS<sub>4</sub> has a 100% spin-

polarization ratio at Fermi level. Also, for the semiconducting channel, the spin gap and half-metallic band gap are 1.46 eV and 0.44 eV, respectively. It also has a large spin exchange splitting of 0.49 eV in the conduction band. Within the biaxial strain range from -5% to 5%, the ferromagnetic half-metallic properties remain unchanged. Monte Carlo simulations estimate that  $T_c$  for single-layer MnAsS<sub>4</sub> can up to 740 K. The intrinsic half-metallic with high  $T_c$  and excellent stability endows single-layer MnAsS<sub>4</sub> a promising functional material for spintronic applications.

## **5. Acknowledgments**

This work was supported by National Natural Science Foundation of China (No.11904312 and 11904313), the Project of Hebei Educational Department, China (No.ZD2018015 and QN2018012), the Advanced Postdoctoral Programs of Hebei Province (No.B2017003004) and the Natural Science Foundation of Hebei Province (No. A2019203507). Thanks to the High Performance Computing Center of Yanshan University.



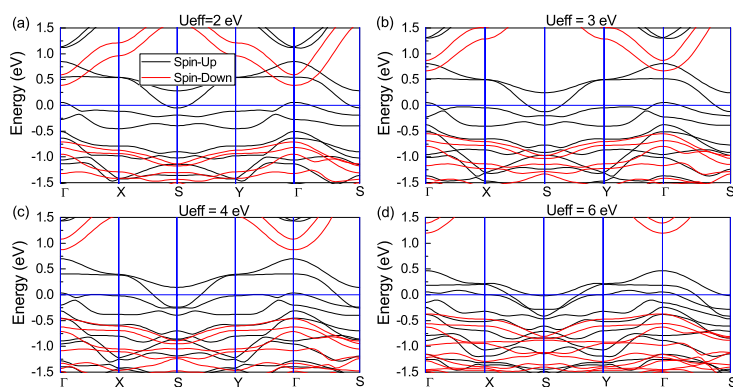


Figure A1: (Color online) The band structures of single-layer MnAsS<sub>4</sub> for different  $U$  values

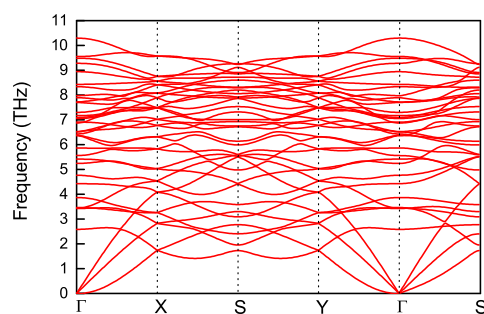


Figure B1: (Color online) Phonon dispersion of single-layer MnAsS<sub>4</sub> obtained from DFT calculations with the PBE functional.

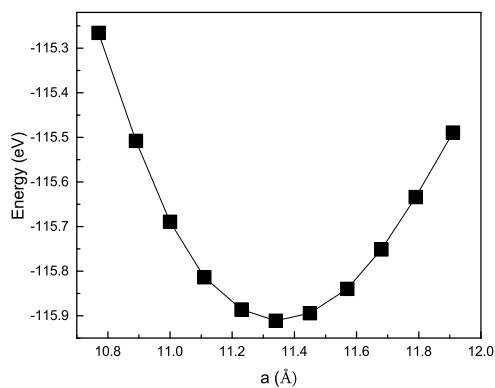


Figure C1: (Color online) Variation of total energy with the lattice constant for single-layer MnAsS<sub>4</sub>.

## References

- [1] Albert Fert. Nobel lecture: Origin, development, and future of spintronics. *Rev. Mod. Phys.*, 80:1517, 2008.
- [2] Xingxing Li and Jinlong Yang. First-principles design of spintronics materials. *Natl. Sci. Rev.*, 3:365, 2016.
- [3] Yuan Ping Feng, Lei Shen, Ming Yang, Aizhu Wang, Minggang Zeng, Qingyun Wu, Sandhya Chintalapati, and Ching-Ray Chang. Prospects of spintronics based on 2D materials. *Wires. Comput. Mol. Sci.*, 7:e1313, 2017.
- [4] Claudia Felser, Gerhard H. Fecher, Fecher, and Benjamin Balke. Spintronics: A challenge for materials science and solid-state chemistry. *Angew. Chem. Int. Ed.*, 46:668, 2007.
- [5] Michael Ashton, Dorde Gluhovic, Susan B. Sinnott, Jing Guo, Derek A. Stewart, and Richard G. Hennig. Two-dimensional intrinsic half-metals with large spin gaps. *Nano. Lett.*, 17:5251, 2017.
- [6] R. A. de Groot, F. M. Mueller, P. G. van Engen, and K. H. J. Buschow. New class of materials: Half-metallic ferromagnets. *Phys. Rev. Lett.*, 50:2024, 1983.
- [7] Bing Wang, Yehui Zhang, Liang Ma, Qisheng Wu, Yilv Guo, Xiwen Zhang, and Jinlan Wang. MnX (X=P, As) monolayers: a new type of two-dimensional intrinsic room temperature ferromagnetic half-metallic material with large magnetic anisotropy. *Nanoscale*, 11:4204, 2019.
- [8] Bo Yang, Junru Wang, Xiaobiao Liu, and Mingwen Zhao. Promising half-metallicity in ductile NbF<sub>3</sub>: a first-principles prediction. *Phys. Chem. Chem. Phys.*, 20:4781, 2018.
- [9] Qisheng Wu, Yehui Zhang, Qionghua Zhou, Jinlan Wang, and Xiao Cheng Zeng. Transition-metal dihydride monolayers: A new family of two-dimensional ferromagnetic materials with intrinsic room-temperature half-metallicity. *J. Phys. Chem. Lett.*, 9:4260, 2018.
- [10] Yungang Zhou, Haifeng Lu, Xiaotao Zu, and Fei Gao. Evidencing the existence of exciting half-metallicity in two-dimensional TiCl<sub>3</sub> and VCl<sub>3</sub> sheets. *Sci. Rep.*, 6:19407, 2016.
- [11] Huan-Huan Xie, Run-Yu Ma, Qiang Gao, Lei Li, and Jian-Bo Deng. Half-metallic ferromagnetism of RbSe and CsTe compounds: A density functional theory study. *Chem. Phys. Lett.*, 661:89, 2016.
- [12] E. Yan. Half-metallic properties in rocksalt and zinc-blende M N (M = Na, K): A first-principles study. *Phys. B*, 407:879, 2012.
- [13] Lei Li, Gang Lei, Qiang Gao, Jian-Bo Deng, and Xian-Ru Hu. First-principles study on the bulk and (111) surface half-metallicity of KS and RbS in CsCl structure. *Mater. Res. Bull.*, 68:308, 2015.
- [14] G. Y. Gao and K. L. Yao. Half-metallic sp-electron ferromagnets in rocksalt structure: The case of SrC and BaC. *Appl. Phys. Lett.*, 91:082512, 2007.
- [15] Houlong L. Zhuang and Jia Zhou. Density functional theory study of bulk and single-layer magnetic semiconductor CrPS<sub>4</sub>. *Phys. Rev. B*, 94:195307, 2016.
- [16] Ting Cao, Zhenglu Li, and Steven G Louie. Tunable magnetism and half-metallicity in hole-doped monolayer GaSe. *Phys. Rev. Lett.*, 114:236602, 2015.
- [17] Muhammad Zulfiqar, Yinchang Zhao, Geng Li, Safdar Nazir, and Jun Ni. Tunable conductivity and half metallic ferromagnetism in monolayer platinum diselenide: a first-principles study. *J. Phys. Chem. C*, 120:25030, 2016.
- [18] P. E. Blöchl. Projector augmented-wave method. *Phys. Rev. B*, 50:17953, 1994.
- [19] G. Kresse and J. Furthmüller. Efficient iterative schemes for ab initio total-energy calculations using a plane-wave basis set. *Phys. Rev. B*, 54:11169, 1996.
- [20] G. Kresse and J. Furthmüller. Efficiency of ab-initio total energy calculations for metals and semiconductors using a plane-wave basis set. *Comput. Mater. Sci.*, 6:15, 1996.
- [21] Hendrik J. Monkhorst and James D. Pack. Special points for brillouin-zone integrations. *Phys. Rev. B*, 13:5188, 1976.
- [22] John P. Perdew, Kieron Burke, and Matthias Ernzerhof. Generalized gradient approximation made simple. *Phys. Rev. Lett.*, 77:3865, 1996.

- [23] A. I. Liechtenstein, V. I. Anisimov, and J. Zaanen. Density-functional theory and strong interactions: Orbital ordering in mott-hubbard insulators. *Phys. Rev. B*, 52:R5467, 1995.
- [24] C. Franchini, R. Podloucky, J. Paier, M. Marsman, and G. Kresse. Ground-state properties of multivalent manganese oxides: Density functional and hybrid density functional calculations. *Phys. Rev. B*, 75:195128, 2007.
- [25] S. L. Dudarev, G. A. Botton, S. Y. Savrasov, C. J. Humphreys, and A. P. Sutton. Electron-energy-loss spectra and the structural stability of nickel oxide: An LSDA + U study. *Phys. Rev. B*, 57:1505, 1998.
- [26] Atsushi Togo and Isao Tanaka. First principles phonon calculations in materials science. *Scr. Mater.*, 108:1, 2015.
- [27] Xingxing Li, Xiaojun Wu, and Jinlong Yang. Half-metallicity in MnPSe<sub>3</sub> exfoliated nanosheet with carrier doping. *J. Am. Chem. Soc.*, 136:11065, 2014.
- [28] Shalini Tomar, Barun Ghosh, Sougata Mardanya, Priyank Rastogi, B.S. Bhadoria, Yogesh Singh Chauhan, Amit Agarwal, and Somnath Bhowmick. Intrinsic magnetism in monolayer transition metal trihalides: A comparative study. *J. Magn. Magn. Mater.*, 489:165384, 2019.
- [29] Tengfei Hu, Wenhui Wan, Yanfeng Ge, and Yong Liu. Strain-tunable magnetic order and electronic structure in 2D CrAsS<sub>4</sub>. *J. Magn. Magn. Mater.*, 497:165941, 2020.
- [30] Zhijian Wu, Erjun Zhao, Hongping Xiang, Xianfeng Hao, Xiaojuan Liu, and Jian Meng. Crystal structures and elastic properties of superhard IrN<sub>2</sub> and IrN<sub>3</sub> from first principles. *Phys. Rev. B*, 76:054115, 2007.
- [31] Fengxian Ma, Mei Zhou, Yalong Jiao, Guoping Gao, Yuantong Gu, Ante Bilic, Zhongfang Chen, and Aijun Du. Single layer bismuth iodide: computational exploration of structural, electrical, mechanical and optical properties. *Sci. Rep.*, 5:17558, 2015.
- [32] Pan Liu, Feng Lu, Maokun Wu, Xiaoguang Luo, Yahui Cheng, Xue-Wei Wang, Weichao Wang, Wei-Hua Wang, Hui Liu, and Kyeongjae Cho. Electronic structures and band alignments of monolayer metal trihalide semiconductors MX<sub>3</sub>. *J. Mater. Chem. C*, 5:9066, 2017.
- [33] G.Y. Gao, Lei Hu, K.L. Yao, Bo Luo, and Na Liu. Large half-metallic gaps in the quaternary heusler alloys CoFeCrZ (Z = Al, Si, Ga, Ge): A first-principles study. *J. Alloy. Compd.*, 551:539, 2013.
- [34] K-I Kobayashi, T Kimura, H Sawada, K Terakura, and Y Tokura. Room-temperature magnetoresistance in an oxide material with an ordered double-perovskite structure. *Nature*, 395:677, 1998.
- [35] Yingjie Sun, Zhiwen Zhuo, Xiaojun Wu, and Jinlong Yang. Room-temperature ferromagnetism in two-dimensional Fe<sub>2</sub>Si nanosheet with enhanced spin-polarization ratio. *Nano. Lett.*, 17:2771, 2017.
- [36] John P. Perdew. Density functional theory and the band gap problem. *Int. J. Quantum Chem.*, 28:497, 1985.
- [37] Yandong Ma, Ying Dai, Meng Guo, Chengwang Niu, Yingtao Zhu, and Baibiao Huang. Evidence of the existence of magnetism in pristine VX<sub>2</sub> monolayers (X = S, Se) and their strain-induced tunable magnetic properties. *ACS. Nano.*, 6:1695, 2012.
- [38] Minwoong Joe, Hosik Lee, M Menderes Alyörük, Jinhwan Lee, Sung Youb Kim, Changgu Lee, and Jun Hee Lee. A comprehensive study of piezomagnetic response in CrPS<sub>4</sub> monolayer: mechanical, electronic properties and magnetic ordering under strains. *J. Phys: Condens. Matter*, 29:405801, 2017.
- [39] Xiaofang Chen, Jingshan Qi, and Daning Shi. Strain-engineering of magnetic coupling in two-dimensional magnetic semiconductor CrSiTe<sub>3</sub>: Competition of direct exchange interaction and superexchange interaction. *Phys. Lett. A*, 379:60, 2015.
- [40] Xingxing Li and Jinlong Yang. CrXTe<sub>3</sub> (X = Si, Ge) nanosheets: two dimensional intrinsic ferromagnetic semiconductors. *J. Mater. Chem. C*, 2:7071, 2014.
- [41] John B. Goodenough. Theory of the role of covalence in the perovskite-type manganites [La,M(II)]MnO<sub>3</sub>. *Phys. Rev.*, 100:564, 1955.

- [42] Junjiro Kanamori. Crystal distortion in magnetic compounds. *J. Appl. Phys.*, 31:S14, 1960.
- [43] M. A. Subramanian, A. P. Ramirez, and W. J. Marshall. Structural tuning of ferromagnetism in a 3D cuprate perovskite. *Phys. Rev. Lett.*, 82:1558, 1999.
- [44] Bevin Huang, Genevieve Clark, Efrén Navarro-Moratalla, Dahlia R Klein, Ran Cheng, Kyle L Seyler, Ding Zhong, Emma Schmidgall, Michael A McGuire, David H Cobden, et al. Layer-dependent ferromagnetism in a van der waals crystal down to the monolayer limit. *Nature*, 546:270, 2017.